The Effect of Solid Interaction Forces on Pneumatic Handling of Sorbent Powders

Rhonda J. Lee and L.-S. Fan
Dept. of Chemical Engineering, The Ohio State University, Columbus, OH 43210

This study shows that a comparison of powder characteristics—particle morphologies, particle size distributions, and static dielectric and Hamaker constants—can be used to interpret differences in dispersion and transport behavior between powders. These differences are attributed to the relative values of the solid-solid interaction forces experienced by each powder in the process. The static dielectric constants of the powders are used as the material properties related to the relative magnitudes of the electrostatic forces. Similarly, the Hamaker constants are the material properties used to indicate the relative magnitudes of the van der Waals forces. The effects of differences in particle morphologies and size distributions are used to evaluate the dispersibility and efficiency of transport of four calcium-based powder materials used as sorbents in flue-gas desulfurization.

Introduction

The solid-solid interaction forces, that is, van der Waals and electrostatic forces, become significant relative to gravity and hydrodynamic forces for fine powder particles in a gas stream. These fine powders are commonly described as Geldart's Group C (cohesive) powders (Geldart, 1972). Group C powders include all powders having a mean particle diameter less than about 30 μm, very wet or sticky materials and powders which agglomerate due to excessive electrostatic charging. The solid-solid interaction forces contribute to inefficient powder handling, that is, powder losses and agglomeration, and consist of both cohesive and adhesive interactions.

Group C dry powder feeding and transport processes are plagued by problems related to the dominating solid-solid interaction forces. Many fine powder dry feeders attempt to disperse or fluidize the powder first (Hamor and Smith, 1971; Davies, 1985; Gullet, 1987; Raghunathan et al., 1992). During gas-solid fluidization, a Group C powder will fluidize inhomogeneously, lifting as a plug or forming cracks and channels. Strong interparticle forces relative to gravity and hydrodynamic forces decrease the ability to disperse or deagglomerate the fine powder particles from a static bulk state. During pneumatic powder transport, an agglomerate that enters the transport system will be less likely to be broken up by the hydrodynamic and impact forces if held together by strong interparticle forces. Also, two dispersed particles that contact each other during transport are more likely to cohere and form an agglomerate if strong interparticle forces exist. Finally, the particles may adhere to the walls of the transport tube where the ease of removal is related to the force of adhesion.

The van der Waals force between two solid materials is due to the electromagnetic interactions of the atoms or molecules making up each solid. The magnitude of the van der Waals force is a function of the interacting atoms or molecules, the distance of separation between solids and the solid-solid contact geometry. An electrostatic force of attraction exists between two oppositely charged solid surfaces. Frictional charging or triboelectrification is responsible for charge generation at powder particle surfaces during dispersion and transport processes. For nonmetallic, resistive powder materials, the charges generated are not easily released to ground or absorbed into the particle material matrix, such as with semiconductor or metallic powder materials. The charges remain "locked" in the particle surfaces, increasing the possibilities for electrostatic interactions.

At particle/particle or particle/wall contact, van der Waals forces are believed to dominate over electrostatic forces (Krupp, 1967; Bailey, 1984; Balachandran, 1987; Visser, 1989). Contact is the equilibrium distance at which the maximum attractive force occurs, arbitrarily set at 4 Å in most studies. This equilibrium distance, however, may actually be a variable, dependent on the contacting materials (Visser, 1981). Electrostatic

Correspondence concerning this article should be addressed to L.-S. Fan.

forces of attraction, on the other hand, are thought to play a role in bringing the particles to the contact point (Krupp, 1967; Balachandran, 1987), relevant to powder transport processes.

The feasibility of obtaining accurate quantitative estimations of the solid-solid interaction forces acting during a powder dispersion and transport process is questionable. Electrostatic charging by triboelectrification is highly variable even when dealing with the same process, and, therefore, difficult if not impossible to predict. The theory of van der Waals forces for solids has made much progress since Hamaker (1937), but the assumption of an ideal contact geometry or surface tension measurements (Visser, 1972) are required before numerical calculation. Estimations of the relative magnitudes of these forces, however, can provide a means to evaluate powders for ease of handling. The evaluation involves making comparisons between powders based on the factors affecting cohesion and adhesion.

Specifically, this approach is used to evaluate the ease of dispersion and transport of Group C calcium-based sorbent powders used for flue-gas desulfurization in coal-fired power plants. The four calcium-based sorbent materials commonly used for flue-gas desulfurization are calcite, dolomite, dolomitic hydrate, and hydrated lime. The calcium in these powders reacts with the sulfur in the flue gas to form solid calcium sulfate. The acceptance of this technology depends on the cost and performance of the calcium-based sorbents used. Increased reactivity is thought to be mainly due to a smaller average particle size and, therefore, greater surface area per volume. The majority of the reaction occurs in the pores of the individual powder particles. Greater powder dispersion results in a smaller average particle size and allows for better access to the particle pores. Access to the particle pores, in turn, decreases the resistance to diffusion of SO_2 through the pore structure and increases the useful surface area for reaction (Gullet, 1987). By evaluating the available sorbents for dispersibility and efficiency of transport, greater performance and lower costs can be realized. In this study, samples of the four sorbent types are characterized and then tested for dispersibility and efficiency of transport. The chemical analyses of the four powders used in this study are shown in Table 1.

The data obtained from the sorbent characterization—particle morphologies, particle size distributions, and Hamaker and static dielectric constants—are used in analyzing the dispersion and transport results. This study attempts to show that with only the relative values of a few parameters related to solid-solid interaction forces, along with a knowledge of the powder particle size distribution and morphology, enough data are available to evaluate powders for dispersibility and efficiency of transport.

Table 1. Material Properties of Sorbents

Chemical Composition wt. %	Calcite	Dolomite	Hydrated Lime	Dolomitic Hydrate
$CaCO_3$	96.4	54.6-55.7	0.35-0.75	—
$MgCO_3$	3.1	44.6-45.8	—	—
$Ca(OH)_2$	—	—	97.0-98.0	63.10
SiO_2	—	0.2-0.3	0.35-0.48	0.80
Al_2O_3	0.33	0.06-0.1	0.15-0.25	0.30
Fe_2O_3	0.07	0.06-0.08	0.05-0.055	0.20
S	1.0	0.01-0.014	0.08-0.098	0.10
MgO	—	—	0.40-0.45	33.50
ρ (g/cm^3)	2.71	2.83	2.23	2.60
ϵ_r	8.20	7.34	13.82	18.64
A ($\times 10^{-20}$) J	9.86	7.34	6.39	7.65

Theory of Solid-Solid Interaction Forces

This section briefly describes the solid-solid interaction force theories used to estimate relative effects. Electrostatic forces are estimated assuming that maximum particle charging occurs, not an unreasonable assumption in pneumatic powder transport processes. Capillary forces are not treated since this study deals only with dry dispersion and transport conditions.

Van der Waals forces

For two plane surfaces, the nonretarded van der Waals force per unit area of contact or pressure is given as (Hamaker, 1937):

$$P_{VDW}=\frac{A}{6\pi H^3} \tag{1}$$

where H is the separation distance and A is referred to as the Hamaker constant. For a sphere of radius R and a plane surface or two spheres of reduced radius R equal to $2R_1R_2/(R_1+R_2)$, the nonretarded approximation gives:

$$F_{VDW}=\frac{AR}{6H^2} \tag{2}$$

Lifshitz (1956) developed the macroscopic theory (also called the modern or continuum theory) of van der Waals forces between solids. He argued that the concept of additivity was unsatisfactory when applied to closely packed atoms in a condensed body. Using the macroscopic theory for two identical solid materials interacting through a vacuum or gas, A can be approximated by (Prieve and Russel, 1987):

$$A=\frac{3\kappa T}{2}\sum_{n=0}^{\infty}{\sum_{s=1}^{\infty}}'\frac{(\Delta^{2s})}{s^3} \tag{3}$$

where

$$\Delta=\frac{\epsilon(i\xi_n)-1.0}{\epsilon(i\xi_n)+1.0} \tag{4}$$

$$\xi_n=n\left(\frac{2\pi\kappa T}{\hbar}\right)\quad n=0,\ 1,\ 2,\ \ldots. \tag{5}$$

and

T = absolute temperature

κ = Boltzman's constant

$\hbar$ = Planck's constant divided by 2 π

The quantity $\epsilon(i\xi_n)$ is related to the complex dielectric permeability, $\epsilon(\omega)$. The complex dielectric permeability, $[\epsilon(\omega)=\epsilon'(\omega)+i\epsilon''(\omega)]$, is a macroscopic property that indicates

the microscopic polarizability of the constituent atoms of a material.

Before A can be determined for a solid material, an expression for $\epsilon(i\xi)$ as a function of ξ_n must be determined. The approach used in this study is to assume that ultraviolet adsorption determines the strength of the van der Waals interaction (Hough and White, 1980) so that

$$\epsilon(i\xi) = 1.0 + \frac{C_{UV}}{1.0 + \left(\frac{\xi}{\omega_{UV}}\right)^2} \tag{6}$$

where C_{UV} and ω_{UV} are the oscillator strength and frequency, respectively, of the ultraviolet absorption peak for that material. These values are determined by the fact that, for most nonconductors in the visible region, $\epsilon(i\xi) = \eta^2(\omega)$, where $\eta(\omega)$ is the refractive index of the material at visible frequency ω, so that

$$\eta^2(\omega) = 1.0 + \frac{C_{UV}}{1.0 - \left(\frac{\omega}{\omega_{UV}}\right)^2} \tag{7}$$

Using Eq. 7, values for C_{UV} and ω_{UV} can be determined from a plot of $[\eta^2(\omega) - 1]$ vs. $[\eta^2(\omega) - 1)\omega^2]$ called the "Cauchy plot." This plot should be linear with a slope equal to $1/\omega_{UV}^2$ and intercept C_{UV}.

The data necessary for the determination of the parameters C_{UV} and ω_{UV} are at least three values of the refractive index at frequencies in the visible range. This information is tabulated in the literature, such as *The Particle Atlas*, for many common substances, or can be measured.

If the value of the Hamaker constant is desired for a solid with a mixture of components, $\epsilon(i\xi)$ can be determined using the Clausius-Mosetti representation (Hough and White, 1980):

$$\frac{\epsilon(i\xi) - 1}{\epsilon(i\xi) + 2} = \phi\left[\frac{\epsilon_1(i\xi) - 1}{\epsilon_1(i\xi) + 2}\right] + (1 - \phi)\left[\frac{\epsilon_2(i\xi) - 1}{\epsilon_2(i\xi) + 2}\right] \tag{8}$$

where ϕ is the volume fraction of component 1, and $\epsilon_j(i\xi)$ corresponds to that function for the pure component j. Equation 8 can be extended to a solid with more than two components.

The theory described above is used to calculate nonretarded Hamaker constants for the four Group C calcium-based sorbent powders investigated in this study. The range of validity of this theory has been experimentally verified at a minimum separation of 10 Å (Israelachvili and Tabor, 1972) up to 100 Å (Langbein, 1971).

Surface deformation is known to increase van der Waals forces by increasing the area of contact (Krupp, 1967; Dahneke, 1972). The calcium-based sorbents investigated are of high hardness (2–4 Mhos), and surface deformation is assumed negligible.

The effect of surface adsorption on van der Waals forces can have two effects. First, the thickness of the adsorbed layer may increase the distance of separation, H, between the powder particles, thereby decreasing the van der Waals force (Krupp, 1967). Second, if the thickness of the adsorbed layer is greater than the separation distance, the dielectric properties of the adsorbed layer will dominate over the base material in the van der Waals interaction (Langbein, 1969). In this study, the powders are carefully dried to remove any adsorbed moisture prior to dispersion and transport. Dispersion and transport are performed with dry nitrogen or dry air, so adsorption of moisture is assumed negligible and not considered in the analysis of van der Waals forces.

Electrostatic forces

In contrast to van der Waals forces, where the optical properties of the interacting bodies permits calculation, at least for ideal geometries, it is not possible to arrive at a general model based on a few material properties to calculate electrostatic forces. Electrostatic charging is extremely variable showing high sensitivity to impurities and the state of the surface. The electronic energy spectrum on or near the surface can be notably affected by as low as 1% surface coverage of adsorbate ions, such as moisture or oxidizing agents (Krupp, 1967; Bailey, 1984). Any small change in the surface condition has been found to cause large variations in observed effects (Kunkel, 1950).

To theoretically gauge the role of electrostatic forces in the dispersion and transport of different fine powders, a standard approach is required. One means of doing this is to consider the maximum theoretical charging. When surfaces are charged by frictional effects in air, such as during dry powder dispersion and transport, the surface charge density is frequently able to reach the Gaussian limit. The Gaussian limit is the point where the electric field adjacent to the surface reaches the level at which air ionizes and then neutralizes the charge.

Gauss's law states that if a closed surface, S, of any shape, is constructed in a region where an electric field is present, then the surface integral of the normal component of the displacement vector, $\boldsymbol{D}$, over the surface is equal to the net free charge, q, enclosed in the surface (Cross, 1987):

$$\int \boldsymbol{D} \cdot d\boldsymbol{s} = \Sigma q \tag{9}$$

If the medium is air, $\boldsymbol{D} = \epsilon_o \boldsymbol{E}$, where ϵ_o is the permittivity of air and $\boldsymbol{E}$ is the electric field vector normal to the surface. This substitution gives:

$$\int \boldsymbol{E} \cdot d\boldsymbol{s} = (\Sigma q)/\epsilon_o \tag{10}$$

If the particle is a dielectric, the interfacial polarization of the atoms adjacent to the charged surface modifies the surface field. The surface field becomes equal to $p\boldsymbol{E}$ where p is related to the polarizability of the material and is a function of the static dielectric constant, ϵ_r:

$$p = \frac{3\epsilon_r}{(\epsilon_r + 2)} \tag{11}$$

The electric field strength at which air ionizes, E_B, is equal to 3×10^6 V/m. The permittivity of air is 8.8×10^{-12} F/m. Substituting these values into Eq. 10 gives an expression for the maximum charge a particle surface can sustain before the ionization of air:

$$q_{max} = (2.64 \times 10^{-5}) \cdot S \cdot p \quad (12)$$

The maximum electrostatic force possible acting on the charged particle can be calculated from the relation $F_{el} = qE$. Substituting $q = q_{max}$ and $E = E_B$, $F_{el,max}$ equals:

$$F_{el,max} = (7.92 \times 10^{1}) \cdot S \cdot p \quad (13)$$

From this analysis, it is concluded that the maximum theoretical electrostatic force acting on a particle is shown to be a function of the surface area of the particle and the particle material's static dielectric constant. In a way similar to the Hamaker constant, the static dielectric constant appears to be a material property that relates to the relative magnitude of the electrostatic forces between materials.

A limitation of Eq. 13 is that the derivation assumes that the charge is uniformly distributed over the surface of the particle. A uniform surface charge will exist if the particle is spherical, having a constant surface curvature. Since most powder materials are of nonuniform shape, this effect on the analysis should be considered. Regions of higher than average curvature will support higher than average surface charge densities. The result will be greater than average electrostatic forces felt in regions of high curvature, such as at the corners of angular particles or at surface asperities.

Experimental Studies

Powder characterization

Particle Morphology. Since the geometry of the contact point affects both the magnitude of the van der Waals forces and the distribution of electrostatic charge, the particle morphology is an important powder characteristic to be considered in the analysis. Scanning electron microscopy (SEM) yields high-resolution images of a specimen surface, making it an ideal technique for investigating particle surface morphologies of powders. This technique is used to evaluate and compare particle morphologies of the four sorbents.

Size Distribution. The magnitudes of the solid-solid interaction forces are found to depend on the size or surface area of the particles interacting. Therefore, when comparing the relative magnitudes of forces between different powders, the difference in average size and the distribution of sizes around the average is important. One problem with comparing experimentally determined particle size distributions between powders is that the resulting distributions are a function of powder density and morphology. Both effects must be considered when comparing size distributions between different powders.

The particle size distributions for each powder are measured with a Sedigraph 5100 V3.02, an instrument that measures sedimentation rates. The Sedigraph analysis is the preferred method for fine powders (Halldin, 1984), because it gives the primary particle size distribution data which are as accurate as experimentally possible. The Sedigraph results consist of plots of the cumulative volume percent vs. aerodynamic diameter for each sorbent powder. In this study, the Sedigraph distribution will be used as a benchmark for comparing the dispersibility of the sorbent powders.

Static Dielectric and Hamaker Constants. The static dielectric constants of the sorbent materials are used to give one indication of the relative magnitudes of the electrostatic forces between powders. The values for calcite and dolomite are taken from the *Handbook of Chemistry and Physics*. The values for hydrated lime and dolomitic hydrate are not available in the literature and have to be measured. These values are obtained by taking capacitance measurements on pressed powder pellets.

Values of the Hamaker constant are determined from optical data—refractive index as a function of frequency in the visible range—for each sorbent. The refractive indices of materials are commonly measured at three wavelengths: C (red, 656 mμ), D (yellow, 589 mμ), and F (blue, 486 mμ). These values, which are normally tabulated, provide the minimum requirement (three measurements) for the Hamaker constant determination.

Calcite, dolomite and hydrated lime are birefringent materials, having uniaxial crystals with two major optic axes, and therefore two reported values of indices of refraction per frequency. Average values are calculated as two thirds the ordinary values plus one third the extraordinary values.

The refractive indices as a function of these three frequencies for calcite and dolomite were measured rather than using tabulated values. These measurements were performed to assure greater accuracy, since tabulated values were found to vary significantly depending on the source (for example, McCrone and Delly, 1973 vs. Winchell and Winchell, 1951). The hydrated lime used in this study was found to be in the crystalline from of epezite, and the values for this material were also measured. The refractive indices of the dolomitic hydrate tested in this study could not be measured, because the average particle size was too small. In this case, Eq. 8 was used for the two components: hydrated lime ($Ca(OH)_2$) and periclase (MgO).

Powder dispersion and transport

The experiments used to test the dispersion and transport properties of the four sorbent materials are described. The transport experiments are performed with two different transport systems designated as transports I and II. Both transport experiments are operated under the condition of dilute solid-gas pneumatic transport.

Dispersion. The dispersion experiments are performed using the AeroSizer particle measuring system (Amherst Process Instruments, Hadley, MA) with a dry powder disperser. With this instrument, a sample of powder is placed in a small cup. The dry disperser uses a pulsed jet to carry the powder particles out of the sample cup and into the carrier gas flow stream. The particles are then impacted upon a disperser pin to break up agglomerates. Finally, the gas-solid dispersion is carried into the sensing unit for particle sizing. The particle sensing unit is two laser beams between which end particle's time of flight is measured and converted into a particle diameter.

With the AeroSizer system, the powders are dispersed dry, and therefore the degree of dispersion can be correlated with the magnitude of the interparticle forces relative to the energy input for dispersion. The disperser conditions (flow and pulse pressure) are preset and computer-controlled. The disperser flow pressure, which controls the carrier gas flow stream to the disperser pin, is kept constant throughout the measurement. The pulse jet pressure, which lifts the particles from the sample cup into the carrier gas stream, is automatically incre-

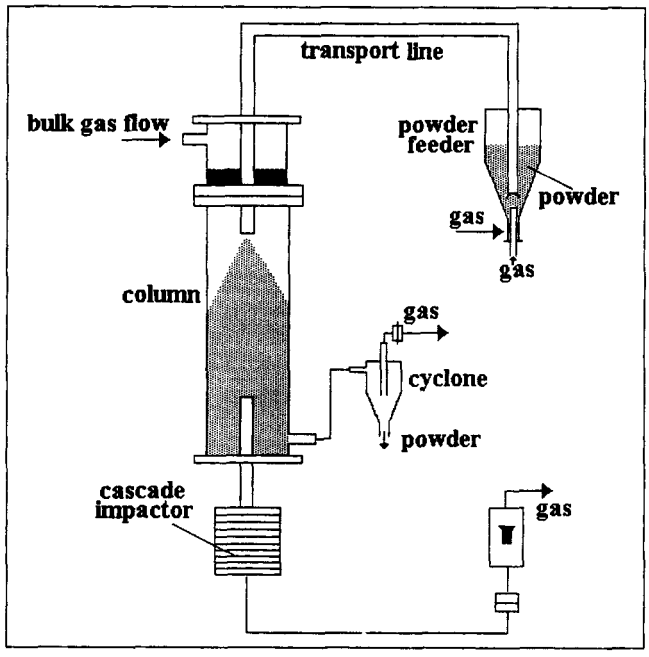

Figure 1. Transport I experimental apparatus.

mented with a feedback system to maintain the particle count rate in a preset range. The majority of the powder dispersion is assumed to occur with the impingement on the disperser pin. Therefore, as long as the disperser flow pressure is the same for all experiments, the energy input for dispersion is assumed to be essentially equal for all experiments.

The dispersion experiments are conducted in the following manner. Each of the four sorbents is tested by placing a small mass of powder in the sample cup and, under the same carrier gas flow pressures, dispersed into the measurement region. These experiments assume that, for the same energy input, the degree of sorbent dispersion should be related to the interparticle forces acting between particles. Each dispersion experiment is fast ($\approx$1 min or less) so that many tests can be run quickly to determine repeatability without worrying about surface contamination with moisture. The results are plotted as cumulative volume percent vs. aerodynamic diameter and directly compared with the Sedigraph results. This comparison is possible since both systems analyze the aerodynamic diameter based on the same basic principle, that is, Newton's law applied to particle motion in a fluid.

Transport I. The experimental apparatus used in the transport I experiments is shown in Figure 1. The powder is dispersed out of the feeder system into a secondary gas stream flowing down the transport tube. The tube material used for all the transport experiments is polyethylene. Polyethylene tubing is chosen as the transport tube due to the ease of removal for cleaning between runs and monitoring powder deposition inside the tube. The gas used in the transport experiments is high-purity nitrogen from a cylinder to assure that moisture into the system is minimal.

As the powder exits the transport tube, it is diluted with dry air in the column. This is required so that the powders can be sampled isokinetically to obtain an accurate particle size distribution. The particle size analyzer used is an Anderson Mark III cascade impactor. The cascade impactor is a multijet, multistage inertial impactor. There are nine jet plates that fractionate the particles into nine aerodynamic size ranges. For more information on cascade impactor principles, see Lodge and Chan (1986).

The feeder system consists of a plexiglas column with a cylindrical top and a conical bottom. Inserted into the bottom region is a 1.2-cm-ID tube fitted with a porous disc. A capillary tube located at the center allows jet flow into the feeder. Gas is fed into the annular region surrounding the capillary tube and flows up through the porous plate. The flow of gas through the porous plate loosens or locally fluidizes the powder in the immediate vicinity. The annular flow is pulsed to provide for better particle loosening. The off-take tube, a 0.63-cm-OD stainless steel tube, is attached to a vibrator to help with particle loosening. More details into this feeder system are presented by Raghunathan et al. (1992).

The four sorbent powders are tested in the transport I apparatus using a 0.32-cm-dia. $\times$ 122-cm-long polyethylene transport tube. The total amount of solids transported for each run can be maintained within the range of approximately $\pm$10% as long as the powder is stirred between runs. With this feeder, however, the solids feed rate cannot be made continuous and feeding is described as pulse feeding. Based on the low mass of powder fed per pulse ($\approx$1.5 mg/pulse, 30 pulses/min) and the high transport velocities, the mode of transport is assumed to be dilute solid-gas pnuematic transport.

The procedure used to test for the transport characteristics of each powder is as follows. First, the particle size distribution out of the feeder is directly measured by attaching the cascade impactor to the feed outlet tube with a short piece of tubing. This distribution is designated as the pretransport size distribution. The posttransport size distribution is measured as the powder exits the transport tube in the cascade impactor using isokinetic sampling.

Transport II. For comparison, the powders are tested in a different transport system. Like in the transport I experiments, the pretransport size distributions, measured directly out of the feeder, are compared with the size distributions measured after powder transport. If both systems give similar findings, there will be greater confidence that the results are material-dependent and not system-dependent.

The transport II system is shown in Figure 2. The polyethylene transport tube dimensions are 0.95 cm in diameter $\times$ 100 cm in length. The volumetric flow of dry air is kept constant at 18 L/min. The particle sizing instrument in this system is the AeroSizer described in the dispersion experiments. The

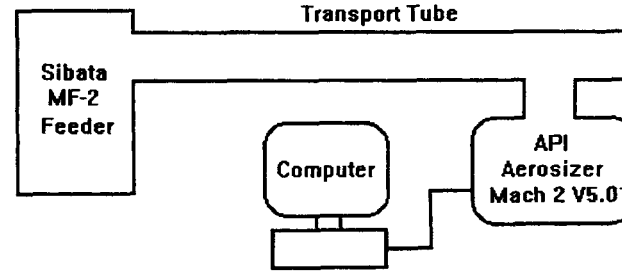

Figure 2. Transport II experimental apparatus.

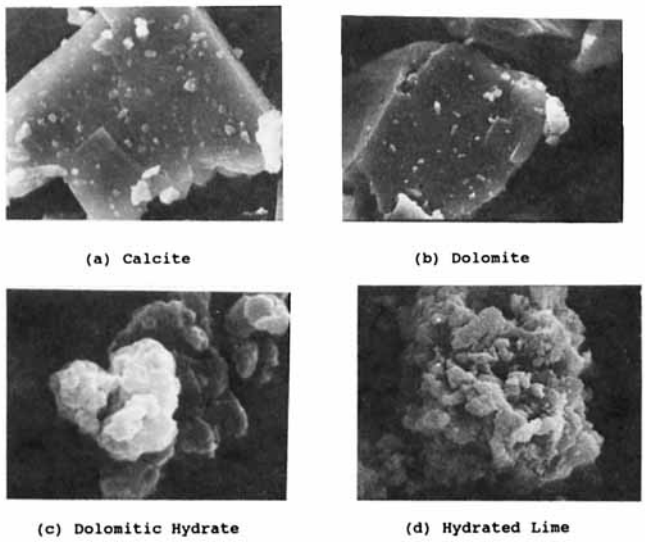

Figure 3. SEM micrographs of four sorbent materials.

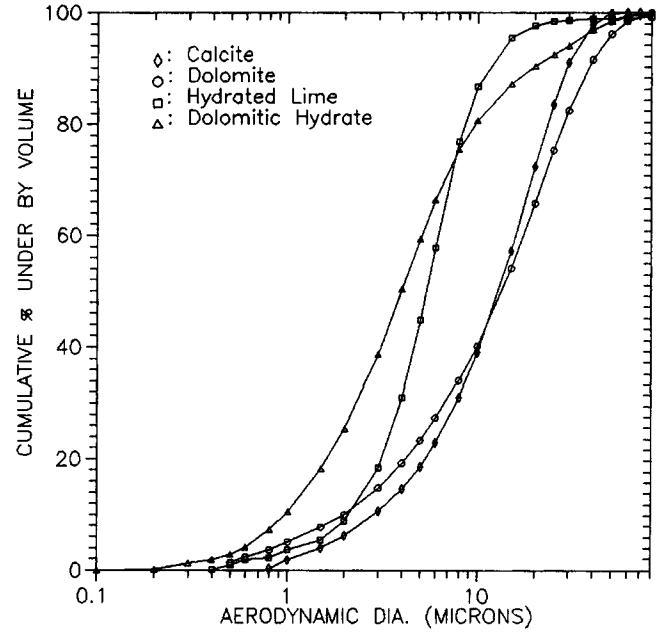

Figure 4. Sedigraph results of four sorbents.

feeder used in this system is a Sibata Micro Feeder MF-2. This feeder supplies a continuous solids feed rate by aspirating solids from grooves in a stainless steel turntable. The ejected particles are then centrifuged in a glass tube to break up agglomerates. The amount of powder in each groove along with the rotation rate of the turntable determines the solids feed rate. The solids feed rate is kept constant at approximately 50 mg/min for each sorbent material, resulting in dilute solid-gas pnuematic transport.

Results

Powder characterization

Scanning Electron Microscopy (SEM). SEM micrographs of the four sorbent materials are shown in Figure 3, which generally indicate the sorbent particle morphologies. The calcite and dolomite (the carbonates) have more angular morphologies than the hydrates. The fine particles of the carbonates ($D \leq 1$ μm) tend to cohere to the flat surfaces of the larger particles (see Figures 3a and 3b).

The hydrates, shown in Figures 3c and 3d, have more rounded morphologies due to their processing from limestones. The individual particles are made up of smaller particles fused together during the hydration process. The results are single particles with rounded surface protrusion or nodules.

Sedigraph. The particle size distributions for the sorbent powders determined from the Sedigraph are shown in Figure 4. The results indicate that directly comparing aerodynamic diameters of calcite and dolomite is reasonable, since the density difference is slight (see Table 1) and the SEM analyses show similar particle morphologies. Figure 4 indicates that calcite and dolomite have comparable median particle sizes, and dolomite has a wider size distribution than the calcite.

Comparing the Sedigraph results for the two hydrates shows the dolomitic hydrate to be composed of finer particles. Though of similar particle morphologies, the difference in densities is greater between these two sorbents than for the carbonates. The effect of a greater density is to increase the aerodynamic diameter reported for a given size. Therefore, the dolomitic hydrate compared to the hydrated lime has an even finer size distribution than is indicated by the Sedigraph.

Static Dielectric and Hamaker Constants. The static dielectric constant of each sorbent material is listed in Table 1. The Cauchy plots generated from the refractive indices data and Eq. 7 are shown in Figure 5 for three of the four sorbent materials and periclase. Table 2 lists the values obtained from the Cauchy plots of the parameters needed for the Hamaker constant determinations. Average values are listed for the uniaxial materials.

The Hamaker constant is calculated for each sorbent material using the values of the parameters in Table 2 combined with Eqs. 3-6. For the dolomitic hydrate, Eq. 7 is solved using refractive indices data for each component, MgO and $Ca(OH)_2$, and the results are used in Eq. 6 to generate $\epsilon_1(i\xi)$ and $\epsilon_2(i\xi)$. Knowing the volume fraction ϕ, Eq. 8 is solved for an average $\epsilon(i\xi)$ at each value of ξ.

The calculated values of the Hamaker constant for the four sorbent materials are listed in Table 1. Calcite has the highest and hydrated lime has the lowest value of the four sorbent materials.

Powder dispersion and transport

Dispersion. The results of the dispersion experiments are shown in Figure 6. For each sorbent tested, the particle size distributions determined with the Sedigraph and AeroSizer are compared. The results presented for the AeroSizer experiments are representative of the majority of individual runs, each run counting at least 200,000 particles. Repeatability between runs was found to be excellent with this instrument. Also included in Figure 6 for each sorbent are the two force constants, A and ϵ_r, as determined in the powder characterization analysis.

The results show that calcite has the least dispersibility, with the majority of the particles having aerodynamic diameters between approximately 15 and 30 μm. For dolomite, the results reveal a greater dispersibility than calcite. The hydrates show

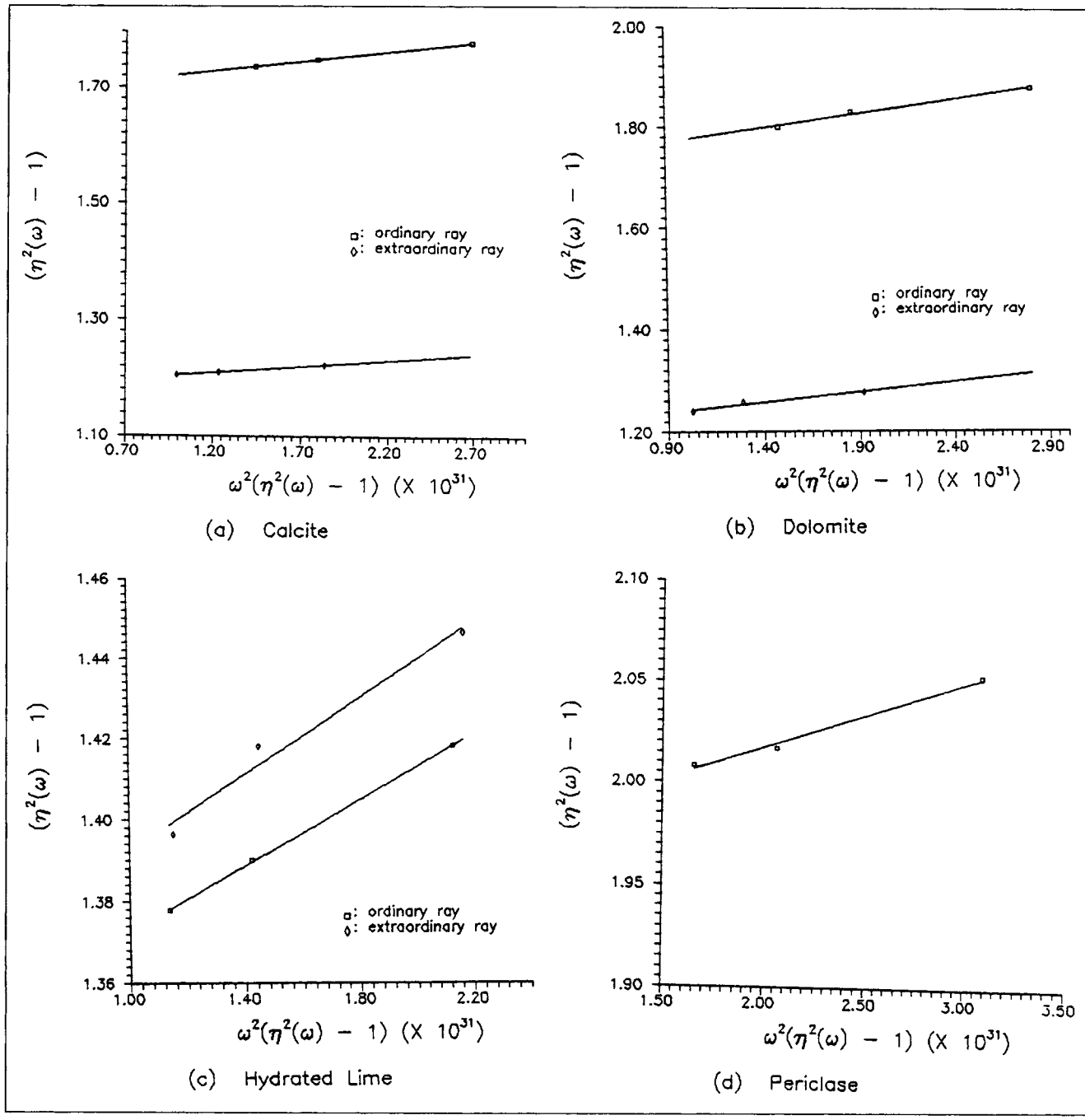

Figure 5. Cauchy plots used in the Hamaker constant determinations.

a very high level of dispersibility. Comparison of the dispersion results for the hydrates indicates that the hydrated lime has a slightly greater dispersibility than the dolomitic hydrate.

Transport I. The transport I results are shown in Figure 7. The pre- and posttransport size distributions are compared in each graph. The two end points (0% and 100%) are not from the impactor, but are approximated from SEM images.

The distributions presented are the average of three runs with approximately the same mass of solid transported per run. The distributions are averaged in this case to lessen the effect of random deviations due to system variability. Also, since the powder flow is not continuous in this system, a solids flow rate is not reported. Particle deposition on the tube wall was observed for all sorbent materials. The transport tube was cleaned after every run to assure the same probability of adhesion between runs.

Figure 7 shows that calcite has a greater difference between size distributions for pre- and posttransport than dolomite. Like calcite, dolomitic hydrate also shows a significant loss of fine particles with transport. The hydrated lime shows essentially no loss of fines above 1 μm, and a small loss of fines less than 1 μm. Comparing the hydrates, the dolomitic hydrate has a much greater coarsening of size with transport than the hydrated lime.

Table 2. Values of Parameters Used in the Hamaker Constant Calculation

Material	$\eta^2(0)$	C_{UV}	ω_{UV} ($\times 10^{16}$)
Calcite			
ordinary ray	2.686	1.686	1.668
extraordinary ray	2.196	1.183	2.171
average	2.523	1.518	1.836
Dolomite			
ordinary ray	1.650	1.722	1.359
extraordinary ray	1.484	1.203	1.604
average	1.595	1.549	1.441
Hydrated Lime			
ordinary ray	2.332	1.332	1.577
extraordinary ray	2.346	1.345	1.461
average	2.337	1.336	1.538
Periclase	2.953	1.953	1.760

Transport II. The results for the transport II system are presented in Figure 8 in histogram form to facilitate Aerosizer instrument's most detailed analysis. They are presented as a number distribution, an instrument option, since the number distribution places more weight on the fine particles, which are influenced most by the solid-solid interaction forces. In other words, by presenting the number distribution, the sensitivity of the results to fine particles is increased. The majority of the particles by number for all sorbent materials are less than 4 μm.

Comparing calcite and dolomite, a similar trend in pre- and posttransport distributions is noted up to the size range 1.2–1.0 μm. For the five ranges between 4.0 and 1.8 μm, the carbonate sorbents show an increase in particle numbers with transport. However, the difference between pre- and post-transport distributions is greater for the calcite. In the ranges

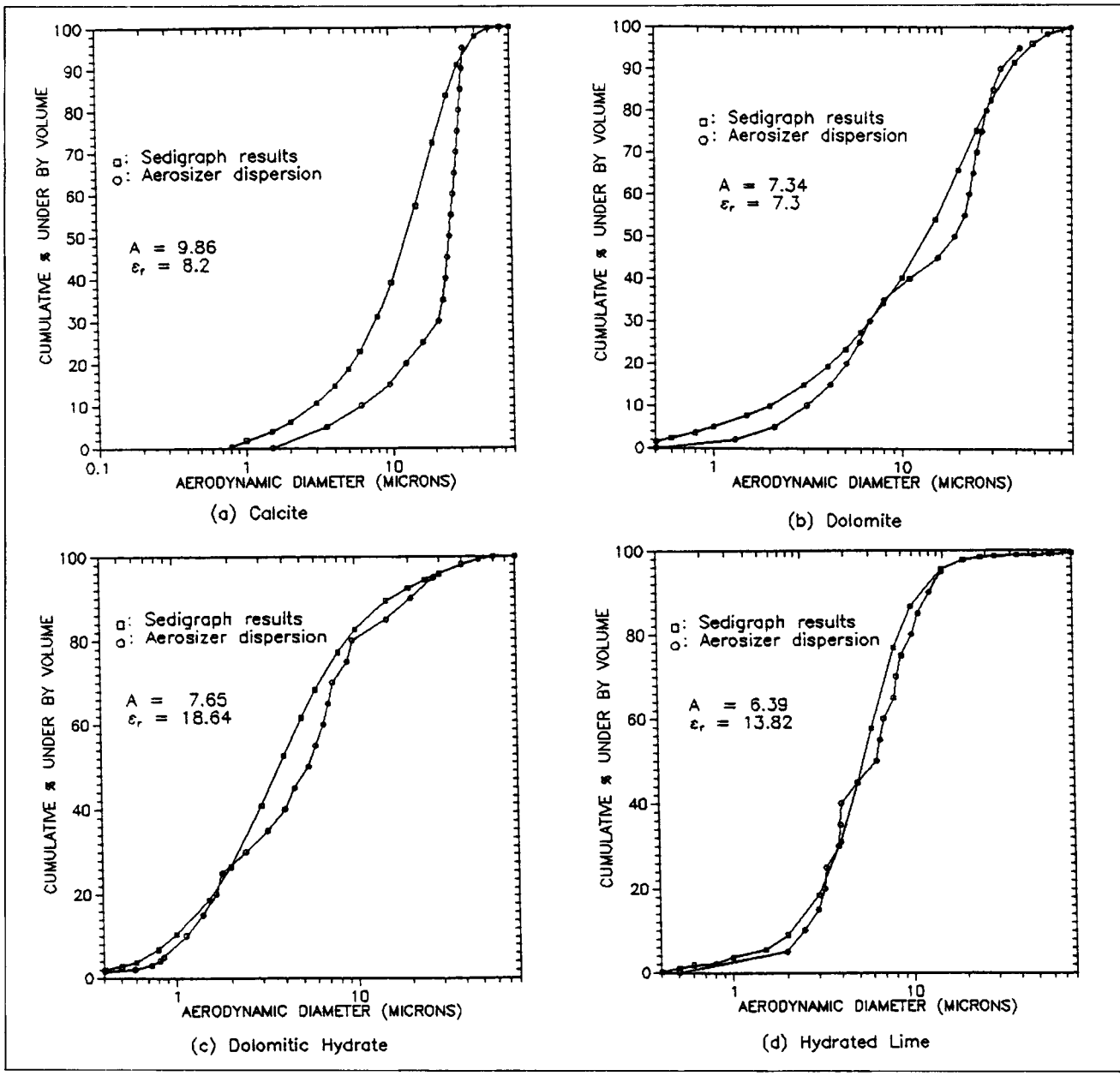

Figure 6. Volume distributions: Aerosizer vs. Sedigraph.

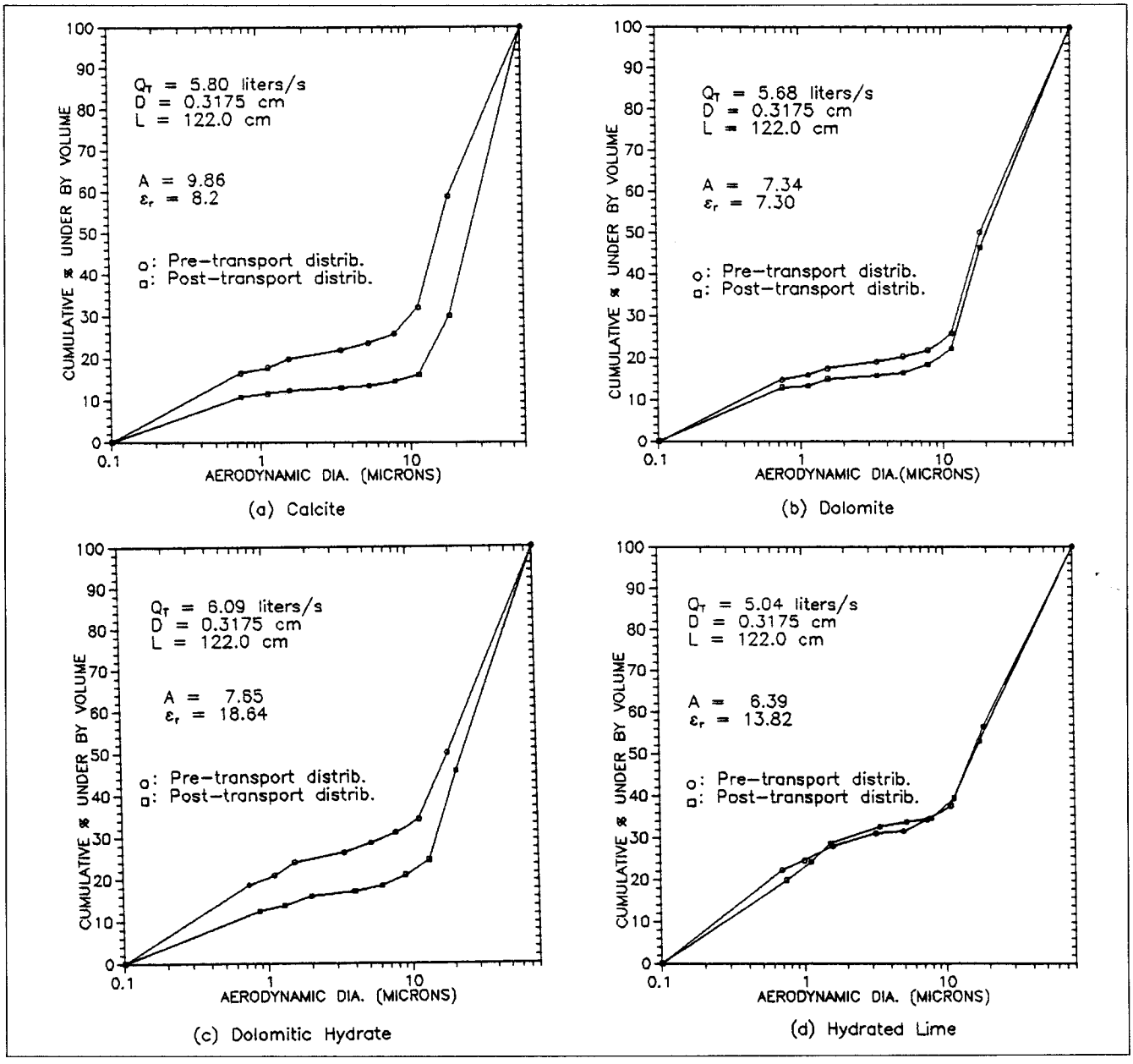

Figure 7. Pre- vs. posttransport volume distributions for the transport I experiments.

below 1.8 μm, the trend reverses in that the post-transport is less than the pretransport number. This shift to larger particle sizes with transport is indicative of the agglomeration/removal of the fine particles. However, in the 1.2–1.0 and 1.0–0.86 μm size ranges, the calcite shows a much greater loss of fines with transport than the dolomite. Particles having $D_a \leq 0.86$ micron are lost during transport for both carbonate powders.

Comparing the hydrates, the dolomitic hydrate, like the calcite, shows a distinct shift toward larger particle sizes with transport. The hydrated lime, on the other hand, shows no clear trend between pre- and posttransport distributions. The results indicate that there may even be deagglomeration occurring with the hydrated lime.

Discussion

In this section, the results from the dispersion and transport experiments are interpreted with respect to the information obtained from the powder characterization analysis.

Powder dispersion and transport

Dispersion. The purpose of the dispersion experiments is to determine how the solid-solid interaction forces affect powder dispersibility. First, the effect of the van der Waals forces will be considered. From the powder characterization results, the calcite is found to have the greatest Hamaker constant and shows the lowest dispersibility in Figure 6. The hydrated lime

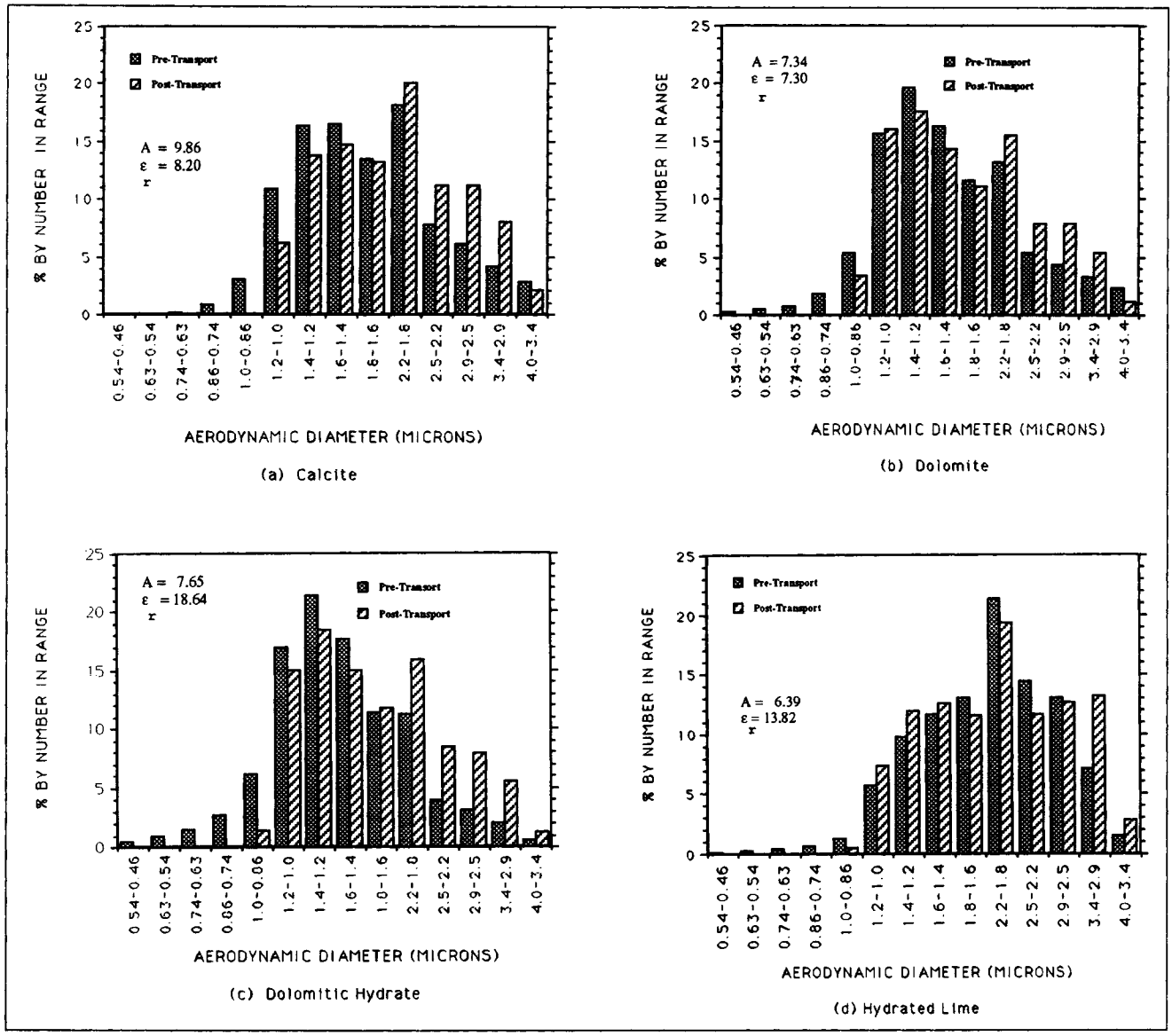

Figure 8. Pre- vs. posttransport number distributions for the transport II experiments.

has the lowest Hamaker constant and shows the greatest dispersibility. However, since contact geometry and particle size also play a role in van der Waals forces, these effects must be considered.

Improvement in the dispersibility of the dolomite over the calcite may be attributed to two interparticle force effects: the lower Hamaker constant and the greater percentage of fine particles. The dolomite has been shown by the Sedigraph analysis to have more fine particles than the calcite. These fine particles are found to cohere to the flat surfaces of the larger particles, as seen in the SEM, acting as spacers between contacting flat surfaces and reducing the van der Waals forces per unit area considerably (as $1/H^3$ for the nonretarded case). The effect is magnified when retardation begins at separations of approximately 0.01 μm, where the van der Waals force decreases as $1/H^4$. Therefore, differences in the dispersibility between the carbonates may be due to two factors, the Hamaker constant and particle size distribution, affecting the relative values of the average van der Waals forces.

Observed differences in the dispersibility between the hydrates are slight. The dolomitic hydrate appears to have a slightly lower dispersibility than the hydrated lime. Again, the difference in the van der Waals forces may be used to explain this observation. Though the average size of the dolomitic hydrate is smaller, the actual value of R used for the van der Waals force calculation should be based on the curvature at the contact point, not the total particle radius as with the electrostatic forces. As seen in the SEM, both hydrate powders are made up of small rounded particles sintered together in the hydration process. The effect of small radii protrusions on the surfaces of each particle, such as in Figures 3c and 3d, results in even smaller average van der Waals forces than if R is based on the total particle radius. The van der Waals forces for the dolomitic hydrate will be slightly greater than for the hydrated lime due to the higher Hamaker coefficient.

The effects of electrostatic forces on dispersibility are evaluated based on the relative values of the dielectric constants with consideration given to the average particle sizes and mor-

phologies, since these factors influence the maximum allowable charging. The dielectric constants of the carbonates are not significantly different, especially when the value of p (see Eq. 11) is compared. Since there is little difference in morphology and average size between calcite and dolomite, the electrostatic forces are expected to be similar for these two materials. Therefore, the observed results may be due to the differences in van der Waals forces alone.

The hydrates show a greater difference between static dielectric constants than the carbonates. However, with the hydrates, the difference in the average particle size must be factored into the analysis. The dolomitic hydrate has a smaller average particle size than the hydrated lime which will offset the effect of the higher static dielectric constant on the relative magnitude of the electrostatic forces. Therefore, it cannot be concluded that higher electrostatic forces are responsible for the slightly lower dispersibility of the dolomitic hydrate.

Greater particle inertia may also play a role in the slightly higher dispersibility of the hydrated lime than the dolomitic hydrate, since inertia has an R^3 dependence. For the carbonates, the effect of inertia should be slight when comparing dispersion results, since the densities and particle sizes are not significantly different.

Comparing all sorbent materials, it appears that the sorbents with the lower average van der Waals forces have greater dispersibility. In addition to the relative magnitudes of the Hamaker constants, differences in contact geometries are suspected of having a significant effect on the relative van der Waals forces. The presence of nodules on the hydrates, as seen in the SEM, results in a reduction of van der Waals forces, and increased dispersion is noted. A greater percentage of fine particles for the dolomite, as determined by the Sedigraph, may be a factor in its increased dispersion. The influence of electrostatic forces on dispersion did not seem significant.

Transport I. As obvious from the results, the van der Waals forces alone cannot explain the observed differences between pre- and posttransport behavior. The dolomitic hydrate shows as much coarsening with transport as the calcite though van der Waals forces are lower as indicated by the Hamaker coefficient and contact geometry. Differences in median diameters are no longer a factor as with dispersion, since pretransport results show all powders to have a median size between 10 and 20 μm prior to transport. When density effects are taken into account, since the results show aerodynamic diameters, even smaller differences in median diameters are observed. This unexpected high level of agglomeration/adhesion observed with the dolomitic hydrate may be due to the increased role of electrostatic forces during the transport process. However, considering the higher efficiency of transport of the hydrated lime compared with the calcite, despite its higher electrostatic forces, may indicate that van der Waals forces may also play a significant role in transport processes.

The van der Waals forces for transport now include not only the particle-particle cohesive interactions but also particle-wall adhesive interactions. A particle more tightly held to the tube wall with greater van der Waals forces will have a smaller probability of being reintroduced into the flow stream. The relative effect of the Hamaker constants and contact geometries on the van der Waals forces will remain unchanged for the case of adherence to the tube wall.

The importance of van der Waals forces to transport processes is also reflected in the comparison of the results between calcite and dolomite. Electrostatic forces are assumed not to be a factor in the observed results based on the similarities in the pretransport average median diameters and static dielectric constants for the carbonates. Random effects are expected to average out. Therefore, the observed difference appears to be due to the difference in the van der Waals forces between the carbonates.

Transport II. The transport II results show some similarity to the transport I results. With this system, however, the differences in pretransport median diameters are greater than those for transport I. This variance is probably due to the better dispersion obtained with this feeder, with the resulting median diameters closer to the primary size values.

The increased agglomeration/loss of fines for both the calcite and dolomitic hydrate with transport is again noted and, as mentioned previously, could be due to the combined effect of van der Waals and electrostatic forces during transport.

Comparing hydrates, the lack of a distinct trend in the hydrated lime results, also seen in transport I, seems to be the effect of lower van der Waals forces reflected in the lower Hamaker constant. As discussed previously, the presence of nodules on the hydrate surfaces acting as the contact points reduces the effect of differences in measured average particle sizes between hydrates on the van der Waals forces. However, it is interesting to note that the electrostatic forces, which should be based on the total particle size, should be similar, if not greater, for the hydrated lime compared to the dolomitic hydrate. The larger average pretransport particle size of the hydrated lime more than offsets the effect of the lower dielectric constant on the theoretically derived equation for the maximum electrostatic forces (Eq. 13). This result may indicate another factor influencing the electrostatic interaction between the hydrates such as nonuniformity of surface charge or a stronger dependence of electrostatic forces on the static dielectric constant than indicated in the theoretical development.

The differences between the carbonate results could be attributed to the effect of lower van der Waals forces for the dolomite, since electrostatic force effects are expected not to be significantly different.

Conclusions

The characterization of powder materials, including particle morphologies, particle size distributions, and static dielectric and Hamaker constants, provides insight into the reasons for differences in dispersion and transport behavior between powders. The theory of interparticle forces indicates that a qualitative comparative analysis of the van der Waals forces between different powders must not be based on the relative values of the material chemcial properties—static dielectric and Hamaker constants—alone, but must include the effects of particle size distributions and particle morphologies.

An analysis of differences in van der Waals and electrostatic forces between the sorbent powders indicates that dispersibility may be controlled by van der Waals forces and that, during transport, both are significant. For the calcium-based sorbent powders investigated in this study, the powder with the lowest Hamaker constant combined with the presence of small, spherical nodules on the surface gives the best dispersion behavior.

For the angular carbonate powders, an increase in the number of fine particles appears to increase both the dispersibility and transport efficiency. The hydrated lime in this study has the best dispersion and transport efficiency of the four sorbents due to the lowest van der Waals forces. The dolomitic hydrate, on the other hand, has good dispersibility but low efficiency of transport. This result is suspected to be due to higher relative electrostatic forces, reflected in the higher dielectric constant.

Acknowledgment

We are indebted to Dr. K. Raghunathan for his design of the apparatus for the transport I experiments. We also wish to thank Gary Laughlin of McCrone Research Institute, Chicago, for measuring refractive indices of the sorbent materials and John Mitchell for his assistance in the SEM analysis.

This work is supported by The Ohio Coal Development Office.

Notation

A = Hamaker constant
C_{UV} = oscillator strength of ultraviolet adsorption peak
D = particle diameter
D_a = aerodynamic particle diameter
D = electric displacement vector
E = electric field vector
E = electric field
E_B = electric breakdown strength of air = 3×10^6 V/m
F_{el} = electrostatic force
F_{VDW} = van der Waals force
$\hbar$ = $6.625 \times 10^{-34}/2\pi$ J·s
H = separation distance between solids
P_{VDW} = van der Waals pressure
q = electric charge
R = particle radius
S = surface area
S = surface vector
T = absolute temperature

Greek letters

ϵ_o = permittivity of air = 8.8×10^{-12} F/m
ϵ_r = static dielectric constant
$\epsilon(\omega)$ = complex dielectric permeability $[\epsilon(\omega) = \epsilon'(\omega) + i\epsilon''(\omega)]$
$\eta(\omega)$ = refractive index at frequency ω
κ = Boltzman's constant = 1.38062×10^{-23} J/K
ξ_n = frequency at energy level n
ϕ = volume fraction
ω = frequency
ω_{UV} = frequency of ultraviolet adsorption peak

Literature Cited

Bailey, A. G., "Electrostatic Phenomena During Powder Handling," *Powder Technology*, **37**, 71 (1984).

Balachandran, W., "Electrostatic Effects in the Adhesion of Particles to Solid Surfaces," *Tribology in Particulate Technology*, Chapter 2.3, B. J. Briscoe and M. J. Adams, eds., Adam Hilger, Bristol and Philadelphia (1987).

Cross, J. A., *Electrostatics: Principles, Problems and Applications*, Adam Hilger, Bristol, 429 (1987).

Dahneke, B., "The Influence of Flattening on the Adhesion of Particles," *J. Colloid Interface Sci.*, **40**(1), 1 (1972).

Davies, T. W., "The Production of Concentrated Powder Suspensions at Low Flow Rates," *Powder Technology*, **42**, 249 (1985).

Geldart, D., "The Effect of Particle Size and Size Distribution on the Behaviour of Gas-Fluidised Beds," *Powder Technology*, **6**, 201 (1972).

Gullet, B. K., "Calcium Hydroxide and Calcium Carbonate Particle Size Effects on Reactivity with Sulfur Dioxide," *Reactivity of Solids*, **3**, 337 (1987).

Halldin, G. W., "Particle Size Analysis of Tungsten Powder," *Powder Technology*, K. Iinoya, J. K. Beddow and G. Limbo, eds., 54 (1984).

Hamaker, H. C., "The London-van der Waals Attraction Between Spherical Particles," *Physica IV*, No. 10, 1058 (Nov. 23, 1937).

Hamor, R. J., and T. W. Smith, "Fluidizing Feeders for Providing Fine Particles at Low, Stable Flows," *Fuel*, **50**(4), 394 (1971).

Hough, D. B., and L. R. White, "The Calculation of Hamaker Constants from Lifshitz Theory with Applications to Wetting Phenomena," *Adv. Colloid Interf. Sci.*, **14**, 3 (1980).

Israelachvili, J. N., and D. Tabor, "The Measurement of van der Waals Dispersion Forces in the Range 1.5 to 130 nm," *Proc. R. Soc. Lond. A*, **331**, 19 (1972).

Kunkel, W. F., "The Static Electrification of Dust Particles on Dispersion into a Cloud," *J. Appl. Phys.*, **21**, 820 (1950).

Krupp, H., "Particle Adhesion Theory and Experiment," *Adv. Colloid Interf. Sci.*, **1**, 111 (1967).

Langbein, D., "Van der Waals Attraction Between Macroscopic Bodies," *J. Adhesion*, **1**, 237 (Oct., 1969).

Langbein, D., "Non-Retarded Dispersion Energy Between Macroscopic Spheres," *J. Phys. Chem. Solids*, **32**, 1657 (1971).

Lifshitz, E. M., "The Theory of Molecular Attractive Force Between Solids," *Soviet Physics*, **2**(1), 73 (Jan., 1956).

Lodge, J. P., and T. L. Chan, eds., *Cascade Impactor, Sampling and Data Analysis*, AIHA, Akron, OH (1986).

McCrone, W. C., and J. G. Delly, eds., *The Particle Atlas, Edition Two: IV*, Ann Arbor Science Publishers, Ann Arbor, MI (1973).

Prieve, D. C., and W. B. Russel, "Simplified Predictions of Hamaker Constants from Lifshitz Theory," *J. Colloid Interf. Sci.*, **125**(1), 1 (Sept., 1988).

Raghunathan, K., A. G. Dastidar, and L.-S. Fan, "A Technique for the Study of Ultrafast Gas-Solid Reactions for Residence Times Less than 100 Milliseconds," *Rev. of Scientific Instr.*, **63**, 5469 (Nov., 1992).

Visser, J., "On Hamaker Constants: A Comparison Between Hamaker Constants and Lifshitz-van der Waals Constants," *Adv. in Colloid and Interf. Sci.*, **3**, 331 (1972).

Visser, J., "The Concept of Negative Hamaker Coefficients: 1. History and Present Status," *Adv. Colloid Interf. Sci.*, **15**, 157 (1981).

Visser, J., "An Invited Review, Van der Waals and Other Cohesive Forces Affecting Powder Fluidization," *Powder Technol.*, **58**, 1 (1989).

Winchell, A. N., and H. Winchell, *Elements of Optical Mineralogy: II. Description of Minerals*, Wiley, New York (1951).

Manuscript received Aug. 24, 1992, and revision received Dec. 14, 1992.